Account of helical and rotational symmetries in the linear augmented cylindrical wave method for calculating the electronic structure of nanotubes: Towards the *ab initio* determination of the band structure of a (100, 99) tubule

P. N. D'yachkov and D. V. Makaev
Kurnakov Institute of General and Inorganic Chemistry, Russian Academy of Sciences, Leninskii Prospekt 31, 119991 Moscow, Russia,
(Received 20 June 2007; revised manuscript received 27 August 2007; published 12 November 2007)

Every carbon single-walled nanotube (SWNT) can be generated by first mapping only two nearest-neighbor C atoms onto a surface of a cylinder and then using the rotational and helical symmetry operators to determine the remainder of the tubule [C. T. White *et al.*, Phys. Rev. B **47**, 5485 (1993)]. With account of these symmetries, we developed a symmetry-adapted version of a linear augmented cylindrical wave method. In this case, the cells contain only two carbon atoms, and the *ab initio* theory becomes applicable to any SWNT independent of the number of atoms in a translational unit cell. The approximations are made in the sense of muffin-tin (MT) potentials and local-density-functional theory only. An electronic potential is suggested to be spherically symmetrical in the regions of atoms and constant in an interspherical region up to the two essentially impenetrable cylinder-shaped potential barriers. To construct the basis wave functions, the solutions of the Schrödinger equation for the interspherical and MT regions of the tubule were sewn together using a theorem of addition for cylindrical functions, the resulting basis functions being continuous and differentiable anywhere in the system. With account of analytical equations for these functions, the overlap and Hamiltonian integrals are calculated, which permits determination of electronic structure of nanotube. We have calculated the total band structures and densities of states of the chiral and achiral, semiconducting, semimetallic, and metallic carbon SWNTs (13, 0), (12, 2), (11, 3), (10, 5), (9, 6), (8, 7), (7, 7), (12, 4), and (100, 99) containing up to the 118 804 atoms per translational unit cell. Even for the (100, 99) system with huge unit cell, the band structure can be easily calculated and the results can be presented in the standard form of four curves for the valence band plus one curve for the low-energy states of conduction band. About 150 functions produce convergence of the band structures better then 0.01 eV independent of the number of atoms in the translational unit cell.

DOI: 10.1103/PhysRevB.76.195411 PACS number(s): 73.22.−f, 73.63.Fg

I. INTRODUCTION

The carbon single-walled nanotubes (SWNTs) are currently the focus of intense multidisciplinary study because of their unique physical and chemical properties and their prospects for practical applications. All the nanotubes can be constructed by rolling up a single graphite sheet, and the structures of SWNTs can be visualized as a conformal mapping of a two-dimensional graphitic lattice onto the surface of a cylinder.[1] One can make such a seamless tubule without any special distortion of their bonding angles other than the introduction of curvature to the carbon hexagons through the rolling process. Each tubule can be labeled by the pair of integers (n_1,n_2) (where $n_1 \geqslant n_2 \geqslant 0$), which, together with C-C bond length $d_{\text{C-C}}$, determine a geometry of the SWNTs (Fig. 1).

The nanotubes generated by the mapping are translationally periodic along the tubule axis, and application of the Bloch theorem facilitates the theoretical studies of the nanotubes band structures.

Theoretical studies of the SWNT electronic structure have received much attention since 1992, when the first calculations for the band structures of nanotubes were done using the tight-binding [linear combination of atomic orbitals (LCAOs)] technique.[2–5] Particularly, it was shown that the electronic structure of any tubule in a region of the occupied and unoccupied π states can be obtained within the tight-binding model by folding the π band along a certain direction in the two-dimensional Brillouin zone of graphene.[1–4] The zone-folding technique has proven immensely successful in providing physically relevant information on the nature of electronic interactions in nanotubes. In this approach, it was predicted that a nanotube is a metal if n_1-n_2 is a multiple of 3, or a semiconductor otherwise.[2–4] Later on, the modified tight-binding π-electron and all-valence orbital band structure models were developed that account for the effects of the π-σ hybridization, misalignment of carbon p_z

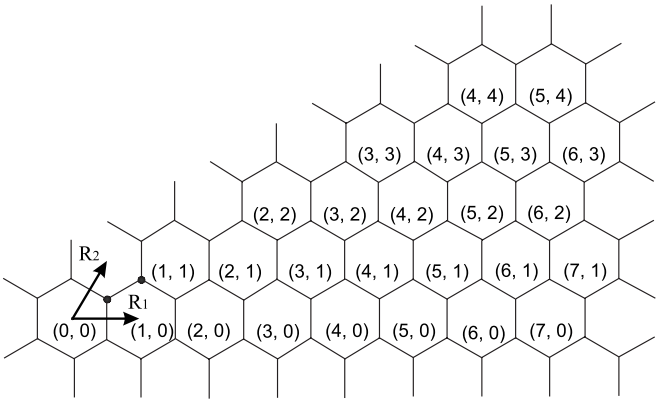

FIG. 1. Graphite layer segment showing indexed lattice points. Nanotubes designated (n_1,n_2) are obtained by rolling the sheet from (0,0) to (n_1,n_2) along a roll-up vector. The chiral angle (from 0° to 30°) is measured between that vector and the zigzag axis.

orbitals on the curved graphene surface, chirality, and diameter dependence of nearest-neighbor hopping integral.[6–13] This leads particularly to modifications of the gap energies, reveals that the SWNTs with $n_1-n_2=3n$ $(n=1,2,\ldots)$ can be very-small-gap semiconductors, and that these effects are of great importance in the case of the small- and moderate-radius nanotubes.[14] Recently, a model based on a symmetry-adapted scheme, with due account of nonorthogonality of the basis set and an empirical calculations of the LCAO parameters using the data for graphite electronic structure, was used for band structure calculations of a number of nanotubes.[15,16]

Including terms causing the trigonal warping effects, similar to the zone-folding technique, results for the highest occupied and lowest unoccupied π states of the SWNTs were obtained using an effective-mass $k\cdot p$ approximation.[17,18]

Going beyond the semiempirical tight-binding methods or $k\cdot p$ approximation, one can perform the first-principles calculations for actual curved-surfaced SWNT. A version of LCAO pseudopotential method in which the core electrons are replaced by the nonlocal norm-conserving pseudopotentials and the valence electrons are treated with a linear combination of multiple-ζ and polarized atomic orbitals was applied in the calculation of the electronic dispersion energies and density of states in the Fermi energy region for several small SWNTs.[19,21]

In the Fermi energy region, the electronic structure of SWNTs was studied using the plane-wave basis and *ab initio* pseudopotential local-density-functional theory (DFT).[20–33] One assumes that predictive power and accuracy of the tight-binding calculations are less robust compared with the *ab initio* DFT methods.[19] Using this *ab initio* method, it was possible to study in more detail the curvature-induced σ- and π-band mixing and the deviations of chemical bonding from the sp^2 hybridization. In particular, these effects were found to alter significantly the electronic structure of narrow nanotubes compared to the predictions of the tight-binding model. In the case of small-diameter insulating nanotubes, where the diameter is less then 1 nm, the strong σ-π rehybridization modified low-lying nondegenerate conduction band states lowering the band gap down to 50%; moreover, the energy bands are shifted by ~0.1 eV relative to the π-electron tight-binding ones even for nanotubes with moderate diameter (between 1 and 1.5 nm).[21,26] Similar effects were observed in the electronic properties of the SWNTs with polygonized cross section calculated within a plane-wave *ab initio* pseudopotential approach.[23] The pseudopotential calculations on the narrow tubes such as (5, 0) revealed total closure of the gap.[24–26]

With account of the translational symmetry, we developed a linear augmented cylindrical wave (LACW) method for calculating the electronic structure of nanotubes.[35–37] The LACW method is just a reformulation for cylindrical multiatomic systems of the linear augmented plane-wave (LAPW) technique[38–40] well known in a theory of bulk materials. The LACW method was successfully used to correlate the minimum energy gaps between the conduction and valence band singularities of the metallic and semiconducting single-walled and double-walled tubules with the nanotube structure and optical absorption spectra.[41–44] The effects of transition metal intercalation on the electronic properties of the carbon and boron-nitride nanotubes, as well as an influence of impurity atoms on the carbon and boron-nitride nanotubes band structure, were studied using this approach too.[35–37,45,46] On the basis of LACW method, a simple model for the electronic structure of SWNTs embedded in a crystal matrix was developed and used to discuss the transport properties of devices with nanotubes encapsulated in a semiconductor crystal.[47,48]

The LACW method, as applied to the nanotubes, has an advantage over the conventional LCAO and plane-wave pseudopotential methods. While low level LCAO calculations are relatively easy to do, improving the accuracy quickly becomes both technically demanding and computationally very expensive.[34] The main concern with approaches of the LCAO method is the transferability of the basis set. Moreover, it is well known from the band structure of bulk materials that the LCAO basis is adequate to achieve good results for the valence band, but not for the conduction band, because this basis does not include the delocalized conducting plane-wave-type functions. The plane-wave pseudopotential calculations suffer from a slow convergence and an unfavorable scaling: The number of basis functions and the time taken to perform such a calculation on a computer increase asymptotically with the cube of the number of atoms.[34] This method is computationally quite cumbersome for calculating the band structure of the chiral tubes without rotational symmetry; hence, the availability of such results in the literature is very limited.[26] The purely delocalized nature of the plane-wave basis set puts obstacles in the way of calculating inner the low-energy states of the valence band, e.g., the nanotube *s* bands.

The basis of the LACW method has both localized and delocalized components. Finally, the main argument for using cylindrical waves is to account for the cylindrical geometry of the nanotubes in an explicit form that offers the obvious advantages. However, all previous LACW calculations were limited by the achiral (n,n) armchair and $(n,0)$ zigzag tubules with a relatively small number of atoms in the minimum translational unit cell. In the case of the chiral tubules even with small diameters, the minimum number of atoms per unit cell can be a very large one. For example, the translational unit cells of the achiral (10, 10) and chiral (10, 9) SWNTs with virtually equal diameters contain 40 and 1084 carbon atoms, respectively. The large number of atoms that can occur in the minimum translational unit cell makes recourse to the other point-group symmetries of these tubules practically mandatory.

Every SWNT can be generated by first mapping only two nearest-neighbor C atoms onto the surface of a cylinder and then using the rotational and helical symmetry operators to determine the remainder of the tubule.[1] Herein, we use these symmetries to develop the symmetry-adapted version of the LACW method. In this case, the cells contain only two carbon atoms, and the theory becomes applicable to any SWNT, including those with screw axis independent of the number of atoms in the translational unit cell. It is very important that the band structure of any tubule can be easily calculated and the results can be presented in the standard form of four curves for the valence band plus one curve for the low-energy states of the conduction band.

II. THEORY

A. Structure of carbon nanotubes

Let us recall how all the graphitic tubules defined by the integers (n_1,n_2) can also be defined in terms of their helical and rotational symmetries.[1,54] In order to construct the carbon SWNT, one has to map the first atom to an arbitrary point T_1 on the cylinder surface, which requires that the position of the second one T_2 be found by rotating this point

$$\Phi_{T_2} = \pi \frac{n_1 + n_2}{n_1^2 + n_2^2 + n_1 n_2} \tag{1}$$

rad about the cylinder axis in conjunction with a translation

$$\delta_{T_2} = \frac{d_{\text{C-C}}}{2} \frac{n_1 - n_2}{(n_1^2 + n_2^2 + n_1 n_2)^{1/2}} \tag{2}$$

along this axis.

Let us map the first C atom to the point with cylindrical coordinates $Z_1=0$, $\Phi_1=0$, and $R_1=R_{NT}$. In this case, the cylindrical coordinates of the second C atom are $Z_2=\delta_{T_2}$, $\Phi_2=\Phi_{T_2}$, and $R_2=R_{NT}$, where

$$R_{NT} = \frac{d_{\text{C-C}}\sqrt{3}}{2\pi}(n_1^2 + n_2^2 + n_1 n_2)^{1/2} \tag{3}$$

is the nanotube radius.

The cylinder axis coincides with a C_n rotational axis for the tubule, where n is the largest common divisor of n_1 and n_2. Thus the positions of these first two atoms can be used to locate $2(n-1)$ additional atoms on the cylinder surface by $(n-1)$ successive $2\pi/n$ rotations about the cylinder axis. Altogether, these $2n$ atoms complete the specification of the helical motif that can then be used to tile the remainder of the tubule by repeated operation of a single screw operation $S(h,\omega)$ representing a translation

$$h = \frac{3d_{\text{C-C}}}{2} \frac{n}{(n_1^2 + n_2^2 + n_1 n_2)^{1/2}} = \frac{3\sqrt{3}d_{\text{C-C}}^2}{4\pi} \frac{n}{R_{NT}} \tag{4}$$

along the cylinder axis in conjunction with a rotation

$$\omega = 2\pi \frac{n_1 p_1 + n_2 p_2 + (n_2 p_1 + n_1 p_2)/2}{n_1^2 + n_2^2 + n_1 n_2} \tag{5}$$

rad about this axis. The angle ω is defined mod 2π, the integer $p_1 \geqslant 0$, and the positive values of integers p_2 are obtained from the equation

$$p_2 n_1 - p_1 n_2 = n. \tag{6}$$

The different sets of pairs p_2 and p_1 correspond to different numberings of the C atoms of the SWNT; for uniqueness, we choose the minimum value of the p_2 and p_1.

The nanotube chiral angle Θ is calculated from the equation

$$\arccos \Theta = \frac{n_1 + (1/2)n_2}{(n_1^2 + n_2^2 + n_1 n_2)^{1/2}}. \tag{7}$$

Finally, the number of atoms N_{tr} in the smallest translational unit cell can be expressed by

$$N_{tr} = 4(n_1^2 + n_2^2 + n_1 n_2)/L_{tr}, \tag{8}$$

where L_{tr} is the largest common factor of $(2n_1+n_2)$ and $(2n_2+n_1)$.

B. One-electron Hamiltonian

In the LACW method, a concept of one-electron orbitals is used, the separate electrons being characterized by wave functions of their own or spin-orbitals. It is assumed that each spin-orbital can be written as product of spatial and spin functions $\Psi_i(\mathbf{r})\alpha$ and $\Psi_i(\mathbf{r})\beta$, where α and β are the wave functions of electrons with spin "up" and "down," respectively. The spatial function $\Psi_i(\mathbf{r})$ is called an orbital. In the LACW method, a study of the electronic structure of nanotube therefore reduces to a study of its orbitals. The $\Psi_i(\mathbf{r})$, together with the corresponding one-electron energies E_i, are found by solving the one-electron Schrödinger equation

$$\hat{H}\Psi_i(\mathbf{r}) = E_i \Psi_i(\mathbf{r}), \tag{9}$$

with effective one-electron Hamiltonian (in atomic Rydberg units)

$$\hat{H} = -\Delta + V. \tag{10}$$

This Hamiltonian contains the kinetic energy operator $-\Delta$ and the operator V describing the summed action on the electron in consideration of all the other electrons in the system and all its nuclei.

C. Symmetry properties of eigenstates of the single-walled nanotubes

In the perfect nanotube with the C_n symmetry, the nuclei are arranged in a regular array described by a set of rotations by the angles $\omega_n t=(2\pi/n)t$ with arbitrary integer t. Therefore, we can introduce the discrete values of a wave vector k_Φ corresponding to the periodic rotation operator and write, using a cylindrical coordinate system Z,Φ,R,

$$\Psi(Z,\Phi + t\omega_n,R) = e^{i\mathrm{k}_\Phi t\omega_n}\Psi(Z,\Phi,R). \tag{11}$$

Substituting $t=n$ and taking into account an equation $\Psi(Z,\Phi+2\pi,R)=\Psi(Z,\Phi,R)$, we obtain that the values of k_Φ are integers and can be written as

$$\mathrm{k}_\Phi = L + nM, \tag{12}$$

where $M=0,\pm 1,\ldots$, and $L=0,1,\ldots,n-1$.

The perfect nanotube, being infinite in the Z direction, is also invariant under the screw $\hat{S}(h,\omega)$ operation representing a translation h along this axis in conjunction with a rotation ω about it.[1] The screw transformations $\hat{S}(h,\omega)$ form an Abelian group isomorphous with the usual translation group $\hat{T}(h)$. Thus, according to Bloch's theorem, the wave function $\Psi(Z,\Phi,R)$ can be characterized by a continuous wave vector K_P,

$$\Psi(Z+th,\Phi+t\omega,R) = e^{i\mathrm{K}_P th}\Psi(Z,\Phi,R), \tag{13}$$

where

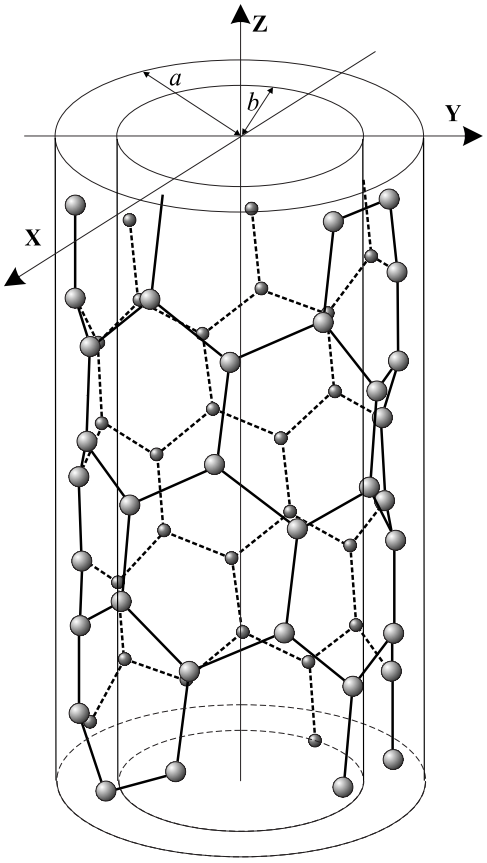

FIG. 2. Atoms of SWNT inside two cylindrical potential barriers.

$$\mathrm{K}_P = \mathrm{k} + \mathrm{k}_P, \quad \mathrm{k}_P = \frac{2\pi}{h}P, \quad P = 0, \pm 1, \ldots . \tag{14}$$

The vectors k belong to the first one-dimensional Brillouin zone—$(\pi/h) < \mathrm{k} \leqslant (\pi/h)$. Note that if $\omega = 2\pi/\mu$ and $h = c/\mu$ with integer μ, where c is the translational lattice constant, then $\mathbf{k} = \mu k$, where k is the traditional one-dimensional (1D) wave vector.

D. Electron potential

In common with the standard and most simple LAPW technique for bulk materials,[38–40] in LACW method, the approximations are made in the sense of muffin-tin (MT) potentials and local-density-functional theory only. However, the electronic potential of a nanotube differs drastically from that of bulk material. Indeed, infinite motion of an electron is possible in any direction in a crystal, but it is obviously limited in the case of nanotubes by their size and shape. In terms of the LACW method, the atoms of nanotube are considered to be enclosed between two essentially impenetrable (in our model, infinite) cylinder-shaped potential barriers Ω_a and Ω_b, because there are two vacuum regions Ω_v on the outside and on the inside of the tubule (Fig. 2).

The radii a and b of these barriers are chosen so that the regions confined by barriers accommodate a significant portion of the electron density of the tubule. Based on our previous calculations of the carbon SWNTs, we take $a = R_{NT} + 2.3$ a.u. and $b = R_{NT} - 2.3$ a.u. (here, R_{NT} is radius of the tubule).

Finally, the electronic potential is spherically symmetrical in the Ω_α regions of MT spheres of atoms α and constant in the interspherical region Ω_{II}. Inside these spheres, we calculate the electron potential by means of the local density approximation with the Slater exchange.[49–51] As usual, the radii of the MT spheres were chosen so that the atomic spheres touch but do not overlap.

In the LACW method, as different from the LAPW approach to bulk materials, the muffin-tin approximation requires an introduction of free parameter, namely, the width of cylindrical layer common for all the carbon SWNTs. This complicates the self-consistent calculations of nanotubes in the terms of the LACW method. Both for the self-consistent and non-self-consistent calculations, the results depend on the choice of this parameter, the best fitted parameters being different in these cases. Particularly, our test self-consistent calculations of the SWNTs using a regular k-point mesh, where seven points were equally spaced between Brillouin zone center and boundary, show that the effect of self-consistency is virtually equivalent to that of a change of the width of a cylindrical layer.

Here, we perform the non-self-consistent calculations of the band structure of the carbon SWNTs in order to avoid this ambiguity in the choice of the width of the cylindrical layer, the electron density of the nanotubes being constructed as the superposition of the atomic ones.

E. Basis functions

To construct the basis wave functions Ψ (LACWs) for SWNT, the solutions of the wave equation for the interspherical and MT regions of the tubule should be sewn together so that the resulting LACWs are continuous and differentiable anywhere in the system.[38–40]

1. Interspherical region

In the interspherical region Ω_{II}, the LACWs are the solutions of the Schrödinger equation for a free electron movement; in the cylindrical coordinates Z, R, Φ, this equation takes the form

$$\left\{ -\left[\frac{1}{R}\frac{\partial}{\partial R} R \frac{\partial}{\partial R} + \frac{1}{R^2}\frac{\partial^2}{\partial \Phi^2} + \frac{\partial^2}{\partial Z^2} \right] + U(R) \right\} \Psi(Z,R,\Phi) = E\Psi(Z,R,\Phi), \tag{15}$$

where

$$U(R) = \begin{cases} 0, & b \leqslant R \leqslant a \\ \infty, & R < b, R > a. \end{cases} \tag{16}$$

Due to cylindrical symmetry of the potential $U(R)$, the solutions of Eq. (15) have the form $\Psi(Z,\Phi,R) = \Psi(Z)\Psi(\Phi)\Psi(R)$. Here, the function

$$\Psi_M(\Phi|L) = \frac{1}{\sqrt{2\pi/n}} \exp[i(L+nM)\Phi] \tag{17}$$

corresponds to a free rotation of an electron in a system with the C_n symmetry. The function

$$\Psi_{P,M}(Z|\mathrm{k},L) = \frac{1}{\sqrt{h}} \exp\left\{ i\left[\mathrm{k} + \mathrm{k}_P - (L+nM)\frac{\omega}{h} \right] Z \right\} \tag{18}$$

corresponds to the free movement of electron along axis Z in an infinite chiral one-dimensional system with the $S(h,\omega)$ screw axis. The coefficients $(2\pi/n)^{-1/2}$ and $h^{-1/2}$ in Eqs. (17) and (18) are determined from normalization conditions

$$\int_0^{2\pi/n} |\Psi_M(\Phi|L)|^2 d\Phi = 1, \tag{19}$$

$$\int_0^{h} |\Psi_{P,M}(Z|\mathrm{k},L)|^2 dZ = 1. \tag{20}$$

The function $\Psi_{|M|,N}(R|L)$ corresponds to the radial movement of an electron in the interspherical regions Ω_{II} of the tubule; it is a solution of the equation

$$\left(-\frac{1}{R}\frac{d}{dR} R \frac{d}{dR} + \frac{(L+nM)^2}{R^2} \right) \Psi_{M,N}(R|L) + U(R)\Psi_{M,N}(R|L) = E_{M,N}(L)\Psi_{M,N}(R|L). \tag{21}$$

Here, $E_{|M|,N}(L)$ is the energy spectrum, and N is the radial quantum number. The energy

$$E_{PMN}(\mathrm{k},L) = \left[\mathrm{k} + \mathrm{k}_P - (L+nM)\frac{\omega}{h} \right]^2 + E_{M,N}(L) \tag{22}$$

corresponds to the wave function $\Psi_{PMN}(Z,R,\Phi|\mathrm{k},L)$. Note that the product $\Psi_M(\Phi|L)\Psi_{P,M}(Z|\mathrm{k},L)$ and, consequently, $\Psi_{PMN}(Z,R,\Phi|\mathrm{k},L)$ satisfy the symmetry conditions (11) and (14). In this equation, the term

$$E(\mathrm{k}) = \left[\mathrm{k} + \mathrm{k}_P - (L+nM)\frac{\omega}{h} \right]^2 = \left[\mathrm{k} + \frac{2\pi}{h}P - \frac{\omega}{h}\mathrm{k}_\Phi \right]^2 \tag{23}$$

determines the energy of free electrons in the 1D empty lattice with screw axis.

Figure 3 shows a dispersion diagram for the special case of the empty lattice with $\omega = 2\pi/3$. Note that the curves are symmetric with respect to a change k for −k, and one can calculate the diagram for the region $0 \leqslant \mathrm{k} \leqslant \frac{\pi}{h}$. It is also instructive to compare this diagram with the dispersion curves of the purely translational 1D empty lattice with $c=3h$ (Fig. 4).

In the regions Ω_{II}, $U(R)=0$ and Eq. (21) takes the form of the Bessel equation:[52,53]

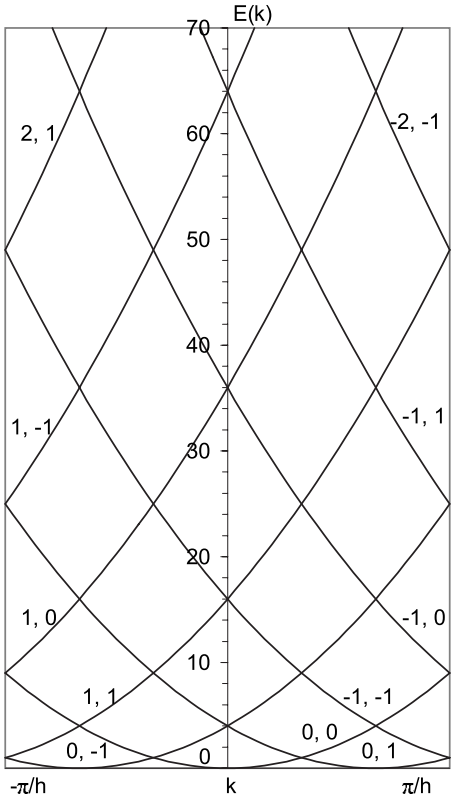

FIG. 3. Dispersion diagram for an empty 1D lattice with screw axis for $\omega = 2\pi/3$. The indices label the values of P and k_Φ, e.g., 2,1 corresponds to dispersion curves with $P=2$ and $\mathrm{k}_\Phi=1$. Energy $E(\mathrm{k})$ is in units of $\left(\frac{\pi}{h}\right)$.

$$\left(\frac{d^2}{dR^2} + \frac{1}{R}\frac{d}{dR} + (\kappa_{|L+nM|,N})^2 - \frac{(L+nM)^2}{R^2} \right) \Psi_{M,N}(R|L) = 0, \tag{24}$$

where $\kappa_{|L+nM|,N} = [E_{M,N}(L)]^{1/2}$. Any solution of this equation is represented by a linear combination of cylindrical Bessel functions of the first J_M and second Y_M kinds,

$$\Psi_{M,N}(R|L) = C^{J,L}_{M,N} J_{L+nM}(\kappa_{|L+nM|,N}R) + C^{Y,L}_{M,N} Y_{L+nM}(\kappa_{|L+nM|,N}R). \tag{25}$$

The function $\Psi_{M,N}(R|L)$ should vanish at $R=a$ and $R=b$,

$$C^{J,L}_{M,N} J_{L+nM}(\kappa_{|L+nM|,N}a) + C^{Y,L}_{M,N} Y_{L+nM}(\kappa_{|L+nM|,N}a) = 0, \tag{26}$$

$$C^{J,L}_{M,N} J_{L+nM}(\kappa_{|L+nM|,N}b) + C^{Y}_{M,L,N} Y_{L+nM}(\kappa_{|L+nM|,N}b) = 0, \tag{27}$$

and be normalized,

$$\int_b^a |\Psi_{M,N}(R|L)|^2 R dR = 1. \tag{28}$$

From Eqs. (26) and (27), we can easily derive the equation for finding $\kappa_{|L+nM|,N}$,

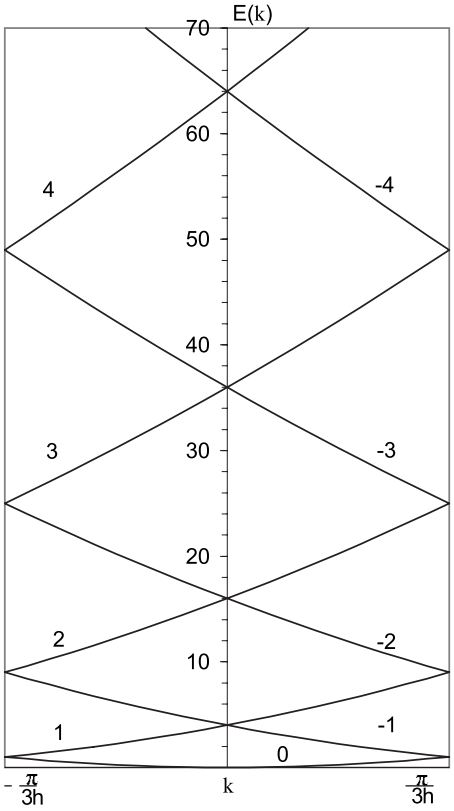

FIG. 4. Triply degenerate dispersion curves for the same system as in Fig. 3, but calculated taking into account only translational symmetry. Account of the screw symmetry results in a shift of some curves. The indices label the values of P. Energy $E(\mathrm{k})$ is in units of $(\frac{\pi}{3h})$.

$$J_{L+nM}(\kappa_{|L+nM|,N}a)Y_{L+nM}(\kappa_{|L+nM|,N}b) = J_{L+nM}(\kappa_{|L+nM|,N}b)Y_{L+nM}(\kappa_{|L+nM|,N}a). \quad (29)$$

In our work, we solve this equation numerically (we determine the segments containing at least one root, which was found by bisecting the segment). From Eqs. (26) and (27), the relationship between $C^{J}_{M,N,L}$ and $C^{Y}_{M,L,N}$ can be found:

$$C^{Y,L}_{M,N} = -C^{J,L}_{M,N}\frac{J_{L+nM}(\kappa_{|L+nM|,N}a)}{Y_{L+nM}(\kappa_{|L+nM|,N}a)}. \quad (30)$$

To calculate integral (28), let us use the equation

$$\int zF_M(\kappa z)G_M(\kappa z)dz = \frac{z^2}{2}F_M(\kappa z)G_M(\kappa z) - \frac{z^2}{4}[F_{M-1}(\kappa z)G_{M+1}(\kappa z) + F_{M+1}(\kappa z)G_{M-1}(\kappa z)] \quad (31)$$

for an indefinite integral and the recurrence formulas

$$zF_{M-1}(z) = zF'_M(z) + MF_M(z), \quad (32)$$

$$-zF_{M+1}(z) = zF'_M(z) - MF_M(z), \quad (33)$$

where F_M and G_M are any two cylindrical functions, in particular, J_M and Y_M. Then,

$$\frac{R^2}{2}[C^{J,L}_{M,N}J'_{L+nM}(\kappa_{|L+nM|,N}R) + C^{Y,L}_{M,N}Y'_{L+nM}(\kappa_{|L+nM|,N}R)]^2|^a_b = 1. \quad (34)$$

Finally, the basis function in the Ω_{II} region in the general cylindrical coordinate system takes the form

$$\Psi_{II,PMN}(Z,\Phi,R|\mathrm{k},L) = \frac{1}{\sqrt{2\pi h/n}}\exp i\left\{\left[\mathrm{k}+\mathrm{k}_P-(L+nM)\frac{\omega}{h}\right]Z+(L+nM)\Phi\right\} \times[C^{J,L}_{M,N}J_{L+nM}(\kappa_{|L+nM|,N}R) + C^{Y,L}_{M,N}Y_{L+nM}(\kappa_{|L+nM|,N}R)]. \quad (35)$$

Here, the $\kappa_{|L+nM|,N}$ values are found from Eq. (29), and $C^{J,L}_{M,N}$ and $C^{Y,L}_{M,N}$ are derived from the set of Eqs. (34) and (30).

Thus, in regions Ω_{II}, the form of the basis function $\Psi_{II,PMN}(Z,\Phi,R|\mathrm{k},L)$ is finally determined. It is a cylindrical wave and

$$\hat{H}\Psi_{II,PMN}(Z,\Phi,R|\mathrm{k},L) = E_{P,M,N}(\mathrm{k},L)\Psi_{II,PMN}(Z,\Phi,R|\mathrm{k},L). \quad (36)$$

2. Muffin-tin region

As in LAPW theory, inside the MT sphere α, the Hamiltonian $\hat{H}=\hat{H}_{MT}$ is spherically symmetric. The radial wave function $u_{l,\alpha}(\rho)$ is taken to be the solution of the radial Schrödinger equation with energy $E_{l,\alpha}$:

$$\hat{H}u_{l,\alpha}(\rho) = E_{l,\alpha}u_{l,\alpha}(\rho). \quad (37)$$

Both in the LAPW and LACW formalisms, $E_{l,\alpha}$ is kept fixed within some energy region. The values of $E_{l,\alpha}$ depend on the nature of atom α. In our calculations of carbon nanotubes, we take $E_0=-14.1$ and $E_1=-5.9$ eV to be equal to the atomic energies of the $2s$ and $2p$ electrons. For E_2 and E_3, we arbitrarily take the values of 10 and 20 eV, respectively; for the E_l with $l\geqslant 4$, we take $E_l=30$ eV. [The results of the linear augmented wave calculations are known to be stable with respect to reasonable variations of the constant-energy parameters $E_{l,\alpha}$ (Refs. 38–40)].

In Rydberg units, Eq. (37) takes the form

$$\frac{1}{\rho}\frac{\partial^2}{\partial\rho^2}(\rho u_{l,\alpha}) + \left[E_{l,\alpha} - V_\alpha(\rho) - \frac{l(l+1)}{\rho^2}\right]u_{l,\alpha} = 0. \quad (38)$$

Here, $V_\alpha(\rho)$ is the local density spherically symmetric potential in the region of the MT sphere α. The functions $u_{l,\alpha}(\rho)$ are normalized inside the MT spheres with radius r_α as

$$\int_0^{r_\alpha} u_{l,\alpha}^2 \rho^2 d\rho = 1,$$

$$\int_0^{r_\alpha} u_{l,\alpha} \hat{H} u_{l,\alpha} \rho^2 d\rho = E_{l,\alpha}. \tag{39}$$

Differentiating Eqs. (37) and (38) with respect to energy yields a differential equation for the radial energy derivative functions $\dot{u}_{l,\alpha}(E_{l,\alpha},\rho) = \partial u_{l,\alpha}(E_{l,\alpha},\rho)/\partial E_{l,\alpha}$:

$$\hat{H}\dot{u}_{l,\alpha}(E_{l,\alpha},\rho) = u_{l,\alpha}(\rho) + E_{l,\alpha}\dot{u}_{l,\alpha}(E_{l,\alpha},\rho), \tag{40}$$

$$\frac{1}{\rho}\frac{\partial^2}{\partial\rho^2}(\rho\dot{u}_{l,\alpha}) + u_{l,\alpha} + \left[E_{l,\alpha} - V_\alpha(\rho) - \frac{l(l+1)}{\rho^2}\right]\dot{u}_{l,\alpha} = 0. \tag{41}$$

The functions $\dot{u}_{l,\alpha}$ and $u_{l,\alpha}$ will be orthogonal as can be seen by differentiating Eq. (39) with respect to energy,

$$\int_0^{r_\alpha} u_{l,\alpha}\dot{u}_{l,\alpha}\rho^2 d\rho = 0 \tag{42}$$

and

$$\int_0^{r_\alpha} u_{l,\alpha}\hat{H}\dot{u}_{l,\alpha}\rho^2 d\rho = 1,$$

$$\int_0^{r_\alpha} \dot{u}_{l,\alpha}\hat{H}u_{l,\alpha}\rho^2 d\rho = 0, \tag{43}$$

$$\int_0^{r_\alpha} \dot{u}_{l,\alpha}\hat{H}\dot{u}_{l,\alpha}\rho^2 d\rho = E_{l,\alpha}N_{l,\alpha},$$

where

$$N_{l,\alpha} = \int_0^{r_\alpha} (\dot{u}_{l,\alpha})^2 \rho^2 d\rho. \tag{44}$$

Multiplying Eq. (38) by $\rho^2\dot{u}_{l,\alpha}$ and Eq. (41) by $\rho^2 u_{l,\alpha}$, subtracting Eq. (41) from Eq. (38), and integrating $\int_0^{r_\alpha} d\rho$ then yield the identity

$$\int_0^{r_\alpha} \rho\left[\dot{u}_{l,\alpha}\frac{\partial^2}{\partial\rho^2}(\rho u_{l,\alpha}) - u_{l,\alpha}\frac{\partial^2}{\partial\rho^2}(\rho\dot{u}_{l,\alpha})\right]d\rho = 1. \tag{45}$$

Moreover, we have

$$\int \rho\left[\dot{u}_{l,\alpha}\frac{\partial^2}{\partial\rho^2}(\rho u_{l,\alpha}) - u_{l,\alpha}\frac{\partial^2}{\partial\rho^2}(\rho\dot{u}_{l,\alpha})\right]d\rho = \rho^2\left(\dot{u}_{l,\alpha}\frac{\partial}{\partial\rho}u_{l,\alpha} - u_{l,\alpha}\frac{\partial}{\partial\rho}\dot{u}_{l,\alpha}\right). \tag{46}$$

Finally, from Eqs. (45) and (46), we obtain[38–40]

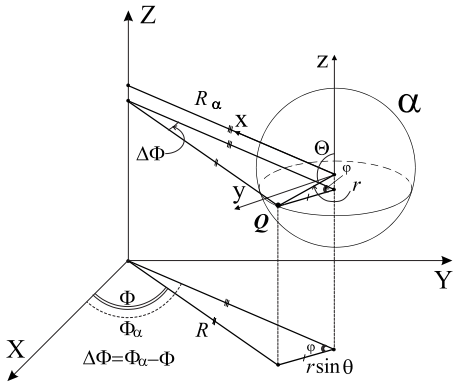

FIG. 5. General cylindrical and local spherical coordinate systems.

$$\rho^2\left[\dot{u}_{l,\alpha}(\rho)u'_{l,\alpha}(\rho) - u_{l,\alpha}(\rho)\dot{u}'_{l,\alpha}(\rho)\right]\big|_{\rho=r_\alpha} = 1, \tag{47}$$

where $u'_{l,\alpha} = \partial u_{l,\alpha}/\partial\rho$ and $\dot{u}'_{l,\alpha} = \partial\dot{u}_{l,\alpha}/\partial\rho$ are radial derivatives of the $u_{l,\alpha}$ and $\dot{u}_{l,\alpha}$ functions.

Following the LAPW theory,[38–40] inside the muffin-tin spheres (Ω_l), the basis function $\Psi_{I,PMN}(\mathrm{k},L)$ can be now written as a linear combination of spherical solutions. In the local spherical coordinate system ρ,θ,φ, the LACW $\Psi_{PMN}(\mathrm{k},L)$ is expanded in spherical harmonics $Y_{lm}(\theta,\varphi)$:

$$\Psi_{I\alpha,PMN}(\rho,\theta,\varphi|\mathrm{k},L) = \sum_{l=0,}^{\infty}\sum_{m=-l}^{l}\left[A_{lm,\alpha}u_{l,\alpha}(E_{l,\alpha},\rho) + B_{lm,\alpha}\dot{u}_{l,\alpha}(E_{l,\alpha},\rho)\right]Y_{lm}(\theta,\varphi). \tag{48}$$

Coefficients $A_{lm,\alpha}$ and $B_{lm,\alpha}$ are selected so that both the LACW $\Psi_{PMN}(\mathrm{k},L)$ and its derivative have no discontinuities at the boundaries of the MT spheres.

3. Sewing conditions

To do this, let us express the $\Psi_{II,PMN}$ function [Eq. (35)] through the cylindrical coordinates Z_α, Φ_α, and R_α of the center of the αth sphere and through the local spherical coordinate system ρ, θ, and φ (Fig. 5).

Let $Q = Q(Z,\Phi,R)$ be the point with coordinates Z, Φ, and R in the general cylindrical coordinate system and with coordinates ρ, θ, and φ in the local spherical coordinate system. Then, taking into account $Z = Z_\alpha + \rho\cos\theta$ and $\Delta\Phi = \Phi_\alpha - \Phi$, we have

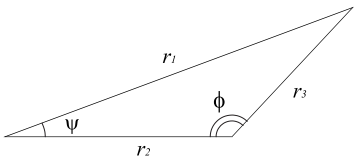

FIG. 6. Illustration to the theorem of addition.

$$\Psi_{II\alpha,PMN}(Z,\Phi,R|\mathrm{k},L)=\frac{1}{\sqrt{2\pi h/n}}\exp\left\{i\left[\left(\mathrm{k}+\mathrm{k}_P-(L+nM)\frac{\omega}{h}\right)Z_\alpha+(L+nM)\Phi_\alpha\right]\right\}$$
$$\times\exp\left\{i\left[\mathrm{k}+\mathrm{k}_P-(L+nM)\frac{\omega}{h}\right]\rho\cos\theta\right\}\exp[-i(L+nM)\Delta\Phi][C^{J,L}_{M,N}J_{L+nM}(\kappa_{|L+nM|,N}R)$$
$$+C^{Y,L}_{M,N}Y_{L+nM}(\kappa_{|L+nM|,N}R)]. \quad (49)$$

In order to write finally this equation in terms of the ρ,θ,φ, coordinates, one has to eliminate the cylindrical coordinates R and $\Delta\Phi$. To achieve this objective, one has to use the theorem of addition (expansion) for cylindrical functions F_M (Fig. 6),[52,53] according to which

$$e^{iM\psi}F_M(\kappa r_1)=\sum_{m=-\infty}^{\infty}J_m(\kappa r_3)F_{m+M}(\kappa r_2)e^{im\varphi}, \quad (50)$$

where F_M is the cylindrical Bessel functions of the first (J_M) or second (Y_M) kind and κ is an arbitrary complex number.

Therefore, we can write

$$e^{-i(L+nM)\Delta\Phi}F_{L+nM}(\kappa_{|L+nM|,N}R)=(-1)^{(L+nM)}\sum_{m=-\infty}^{\infty}J_m(\kappa_{|L+nM|,N}\rho\sin\theta)F_{m-(L+nM)}(\kappa_{|L+nM|,N}R_\alpha)e^{im\varphi}. \quad (51)$$

Finally, the function $\Psi_{II\alpha,PMN}(Z,\Phi,R|\mathrm{k},L)$ takes the form

$$\Psi_{II\alpha,PMN}(Z,\Phi,R|\mathrm{k},L)=\frac{1}{\sqrt{2\pi h/n}}\exp\left\{i\left[\left(\mathrm{k}+\mathrm{k}_P-(L+nM)\frac{\omega}{h}\right)Z_\alpha+(L+nM)\Phi_\alpha\right]\right\}\exp\left\{i\left[\mathrm{k}+\mathrm{k}_P-(L+nM)\frac{\omega}{h}\right]\rho\cos\theta\right\}$$
$$\times(-1)^{(L+nM)}\sum_{m=-\infty}^{\infty}[C^{J,L}_{M,N}J_{m-(L+nM)}(\kappa_{|L+nM|,N}R_\alpha)+C^{Y,L}_{M,N}Y_{m-(L+nM)}(\kappa_{|L+nM|,N}R_\alpha)]$$
$$\times J_m(\kappa_{|L+nM|,N}r\sin\theta)\exp(im\varphi). \quad (52)$$

From the equality of the $\Psi_{I\alpha,PMN}$ and $\Psi_{II\alpha,PMN}$ functions and of their derivatives at the sphere boundary, we have

$$A_{lm,\alpha}=r_\alpha^2D(\mathrm{k},L)^{PMN}_{lm,\alpha}a^{PMN}_{lm,\alpha}(r_\alpha), \quad (53)$$

$$B_{lm,\alpha}=r_\alpha^2D(\mathrm{k},L)^{PMN}_{lm,\alpha}b^{PMN}_{lm,\alpha}(r_\alpha). \quad (54)$$

Here, r_α is a radius of MT sphere of atom α,

$$D(\mathrm{k},L)^{PMN}_{lm,\alpha}=\frac{1}{\sqrt{2h/n}}\left\{\frac{(2l+1)[(l-|m|)!]}{[(l+|m|)!]}\right\}^{1/2}$$
$$\times(-1)^{[0.5(m+|m|+l)]}i^l\exp i\left\{\left[\mathrm{k}+\mathrm{k}_P-(L+nM)\frac{\omega}{h}\right]^2Z_\alpha+(L+nM)\Phi_\alpha\right\}(-1)^{(L+nM)}$$
$$\times[C^{J,L}_{M,N}J_{m-(L+nM)}(\kappa_{|L+nM|,N}R_\alpha)+C^{Y,L}_{M,N}Y_{m-(L+nM)}(\kappa_{|L+nM|,N}R_\alpha)], \quad (55)$$

$$a^{PMN}_{lm,\alpha}(r_\alpha)=I^{PMN}_{2,\alpha}(r_\alpha)\dot{u}_{l,\alpha}(r_\alpha)-I^{PMN}_{1,\alpha}(r_\alpha)\dot{u}'_{l,\alpha}(r_\alpha), \quad (56)$$

$$b^{PMN}_{lm,\alpha}(r_\alpha)=I^{PMN}_{1,\alpha}(r_\alpha)u'_{l,\alpha}(r_\alpha)-I^{PMN}_{2,\alpha}(r_\alpha)u_{l,\alpha}(r_\alpha). \quad (57)$$

Finally, I_1 and I_2 are integrals of the augmented Legendre polynomials $P_l^{|m|}$:

$$I_1=2\int_0^{\pi/2}\exp\left\{i\left[\left(\mathrm{k}+\mathrm{k}_P-(L+nM)\frac{\omega}{h}\right)r_\alpha\cos\theta\right]\right\}$$
$$\times J_m(\kappa_{|L+nM|,N}r_\alpha\sin\theta)P_l^{|m|}(\cos\theta)\sin\theta d\theta, \quad (58)$$

$$I_2=2\int_0^{\pi/2}\exp\left\{i\left[\left(\mathrm{k}+\mathrm{k}_P-(L+nM)\frac{\omega}{h}\right)r_\alpha\cos\theta\right]\right\}$$
$$\times\left[i\left(\mathrm{k}+\mathrm{k}_P-(L+nM)\frac{\omega}{h}\right)\cos\theta J_m(\kappa_{|L+nM|,N}r_\alpha\sin\theta)\right.$$
$$\left.+(1/2)\kappa_{|L+nM|,N}\sin\theta\right][J_{m-1}(\kappa_{|L+nM|,N}r_\alpha\sin\theta)$$
$$-J_{m-1}(\kappa_{|L+nM|,N}r_\alpha\sin\theta)]P_l^{|m|}(\cos\theta)\sin\theta d\theta. \quad (59)$$

F. Overlap integrals and Hamiltonian matrix elements

Due to symmetry conditions, the overlap and Hamiltonian integrals are equal to *zero*,

$$\int_{\Omega} \Psi^{*}_{P_2M_2N_2}(\mathbf{r}|\mathrm{k}_2,L_2)\Psi_{P_1M_1N_1}(\mathbf{r}|\mathrm{k}_1,L_1)dV=0, \quad (60)$$

$$\int_{\Omega} \Psi^{*}_{P_2M_2N_2}(\mathbf{r}|\mathrm{k}_2,L_2)\hat{H}\Psi_{P_1M_1N_1}(\mathbf{r}|\mathrm{k}_1,L_1)dV=0, \quad (61)$$

if $\mathrm{k}_2 \neq \mathrm{k}_1$ or $L_2 \neq L_1$.

The integral $\langle \Psi_{P_2M_2N_2}|\Psi_{P_1M_1N_1}\rangle$ of the product of the LACWs $\Psi^{*}_{P_2M_2N_2}$ and $\Psi_{P_1M_1N_1}$ over the unit cell Ω is equal to the integral of the product of cylindrical waves $\Psi^{*}_{II,P_2M_2N_2}$ and $\Psi_{II,P_1M_1N_1}$ over the interspherical regions Ω_{II} plus the sum of the integrals of the product of spherical parts of the LACWs $\Psi^{*}_{I\alpha,P_2M_2N_2}$ and $\Psi_{I\alpha,P_1M_1N_1}$ over the MT regions:

$$\int_{\Omega} \Psi^{*}_{P_2M_2N_2}(\mathbf{r}|\mathrm{k},L)\Psi_{P_1M_1N_1}(\mathbf{r}|\mathrm{k},L)dV=\int_{\Omega_{II}} \Psi^{*}_{P_2M_2N_2}(\mathbf{r}|\mathrm{k},L)\Psi_{P_1M_1N_1}(\mathbf{r}|\mathrm{k},L)dV+\sum_{\alpha}\int_{\Omega\alpha} \Psi^{*}_{P_2M_2N_2}(\mathbf{r}|\mathrm{k},L)\Psi_{P_1M_1N_1}(\mathbf{r}|\mathrm{k},L)dV. \quad (62)$$

The integral over Ω_{II} is equal to the integral over Ω minus the sum of the integrals over the MT regions. Due to the fact that the cylindrical waves as solutions of the Schrödinger equation [Eq. (15)] are orthonormalized, the integral over Ω is equal to the product of the δ functions. As a result, Eq. (62) takes the form

$$\langle \Psi_{P_2M_2N_2}(\mathrm{k},L)|\Psi_{P_1M_1N_1}(\mathrm{k},L)\rangle=\delta_{P_2M_2N_2,P_1M_1N_1}-\sum_{\alpha}\int_{\Omega\alpha}\Psi^{*}_{II,P_2M_2N_2}(\mathbf{r}|\mathrm{k},L)\Psi_{II,P_1M_1N_1}(\mathbf{r}|\mathrm{k},L)dV+\sum_{\alpha}\int_{\Omega\alpha}\Psi^{*}_{I\alpha,P_2M_2N_2}(\mathbf{r}|\mathrm{k},L)\Psi_{I\alpha,P_1M_1N_1}(\mathbf{r}|\mathrm{k},L)dV. \quad (63)$$

With the use of the equations for the $\Psi_{II,PMN}(\mathbf{r}|\mathrm{k},L)$ and $\Psi_{I\alpha,PMN}(\mathbf{r}|\mathrm{k},L)$ functions, we finally obtain the following for the overlap matrix elements:

$$\begin{aligned}\langle \Psi_{P_2M_2N_2}|\Psi_{P_1M_1N_1}\rangle|_{\mathrm{k},L}=\delta_{P_2M_2N_2,P_1M_1N_1}-\frac{n}{h}(-1)^{n(M_2+M_1)}\sum_{\alpha}\exp\left\{i\left[\left(\mathrm{k}_{P_1}-\mathrm{k}_{P_2}-n(M_1-M_2)\frac{\omega}{h}\right)Z_{\alpha}+n(M_1\right.\right.\\ \left.\left.-M_2)\Phi_{\alpha}\right]\right\}\sum_{m=-\infty}^{\infty}[C^{J,L}_{M_2N_2}J_{m-(L+nM_2)}(\kappa_{|L+nM_2|,N_2}R_{\alpha})+C^{Y,L}_{M_2N_2}Y_{m-(L+nM_2)}(\kappa_{|L+nM_2|,N_2}R_{\alpha})]\\ \times[C^{J,L}_{M_1N_1}J_{m-(L+nM_1)}(\kappa_{|L+nM_1|,N_1}R_{\alpha})+C^{Y,L}_{M_1N_1}Y_{m-(L+nM_1)}(\kappa_{|L+nM_1|,N_1}R_{\alpha})]\left\{I^{P_2M_2N_2,P_1M_1N_1}_{3,m\alpha}(r_{\alpha})\right.\\ \left.-r^{4}_{\alpha}\sum_{l=|m|}^{\infty}\frac{(2l+1)[(l-|m|)!]}{2[(l+|m|)!]}S^{P_2M_2N_2,P_1M_1N_1}_{lm,\alpha}(r_{\alpha})\right\},\end{aligned} \quad (64)$$

where

$$I_{3,m\alpha}=2\int_{0}^{\pi/2}\int_{0}^{r_{\alpha}}\cos[r(\mathrm{k}_{P_1}-\mathrm{k}_{P_2})\cos\theta]J_m(\kappa_{|L+nM_2|,N_2}r\sin\theta)J_m(\kappa_{|L+nM_1|,N_1}r\sin\theta)\sin\theta r^2 d\theta dr,$$

$$S_{lm,\alpha}=(a^{P_2M_2N_2}_{lm,\alpha})^{*}a^{P_1M_1N_1}_{lm,\alpha}+N_{l,\alpha}(b^{P_2M_2N_2}_{lm,\alpha})^{*}b^{P_1M_1N_1}_{lm,\alpha}. \quad (65)$$

Analogously, for the Hamiltonian matrix elements of SWNT, we have

$$\int_{\Omega}\Psi^{*}_{P_2M_2N_2}(\mathbf{r}|\mathrm{k},L)\hat{H}\Psi_{P_1M_1N_1}(\mathbf{r}|\mathrm{k},L)dV=\int_{\Omega_{II}}\Psi^{*}_{II,P_2M_2N_2}(\mathbf{r}|\mathrm{k},L)(-\Delta)\Psi_{II,P_1M_1N_1}(\mathbf{r}|\mathrm{k},L)dV+\sum_{\alpha}\int_{\Omega\alpha}\Psi^{*}_{I\alpha,P_2M_2N_2}(\mathbf{r}|\mathrm{k},L)\hat{H}_{MT}\Psi_{I\alpha,P_1M_1N_1}(\mathbf{r}|\mathrm{k},L)dV. \quad (66)$$

Again, the integral over Ω_{II} is equal to the integral over Ω minus the sum of the integrals over the MT regions. In Ω, cylindrical wave $\Psi_{IIf,PMN}$ is the solution of Schrödinger equation [Eq. (15)] with energy $E_{PMN}(\mathrm{k},L)$. As a result, Eq. (66) takes the form

$$\langle \Psi_{P_2M_2N_2}(\mathrm{k},L)|\hat{H}|\Psi_{P_1M_1N_1}(\mathrm{k},L)\rangle = [E_{P_2M_2N_2}(\mathrm{k},L)E_{P_1M_1N_1}(\mathrm{k},L)]^{1/2}\delta_{P_2M_2N_2,P_1M_1N_1} - \sum_{\alpha}\int_{\Omega\alpha}\Psi^{*}_{II,P_2M_2N_2}(\mathbf{r}|\mathrm{k},L) \times(-\Delta)\Psi_{II,P_1M_1N_1}(\mathbf{r}|\mathrm{k},L)dV + \sum_{\alpha}\int_{\Omega\alpha}\Psi^{*}_{I\alpha,P_2M_2N_2}(\mathbf{r}|\mathrm{k},L)\hat{H}_{MT}\Psi_{I\alpha,P_1M_1N_1}(\mathbf{r}|\mathrm{k},L)dV. \quad (67)$$

Finally, with account of analytical equations for the LACWs in the interspherical and MT regions, one obtains

$$\begin{aligned}\langle \Psi_{P_2M_2N_2}|\hat{H}|\Psi_{P_1M_1N_1}\rangle|_{\mathrm{k},L} &= \left[\mathrm{k}+\mathrm{k}_{P_2}-(L+nM_2)\frac{\omega}{h}+\kappa_{|L+nM_2|,N_2}\right]\left[\mathrm{k}+\mathrm{k}_{P_1}-(L+nM_1)\frac{\omega}{h}+\kappa_{|L+nM_1|,N_1}\right]\delta_{P_2M_2N_2,P_1M_1N_1}\\ &-\frac{n}{h}(-1)^{n(M_2+M_1)}\sum_{\alpha}\exp\left\{i\left[\left(\mathrm{k}_{P_1}-\mathrm{k}_{P_2}-n(M_1-M_2)\frac{\omega}{h}\right)Z_{\alpha}+n(M_1\right.\right.\\ &\left.\left.-M_2)\Phi_{\alpha}\right]\right\}\sum_{m=-\infty}^{\infty}[C^{J,L}_{M_2,N_2}J_{m-M_2}(\kappa_{|L+nM_2|,N_2}R_{\alpha})+C^{Y,L}_{M_2,N_2}Y_{m-M_2}(\kappa_{|L+nM_2|,N_2}R_{\alpha})]\\ &\times[C^{J,L}_{M_1,N_1}J_{m-M_1}(\kappa_{|L+nM_1|,N_1}R_{\alpha})+C^{Y,L}_{M_1,N_1}Y_{m-M_1}(\kappa_{|L+nM_1|,N_1}R_{\alpha})]\\ &\times\left\{\left[\mathrm{k}+\mathrm{k}_{P_2}-(L+nM_2)\frac{\omega}{h}\right]\left[\mathrm{k}+\mathrm{k}_{P_1}-(L+nM_1)\frac{\omega}{h}\right]\right. I^{P_2M_2N_2,P_1M_1N_1}_{3,\alpha}\\ &\left.+\kappa_{|L+nM_2|,N_2}\kappa_{|L+nM_1|,N_1}I'^{P_2M_2N_2,P_1M_1N_1}_{3,\alpha}+m^2I^{P_2M_2N_2,P_1M_1N_1}_{4,\alpha}\right.\\ &-r_{\alpha}^4\sum_{l=|m|}^{\infty}\frac{(2l+1)[(l-|m|)!]}{2[(l+|m|)!]}(E_{l,\alpha}S^{P_2M_2N_2,P_1M_1N_1}_{lm,\alpha}(r_{\alpha})+\gamma^{P_2M_2N_2,P_1M_1N_1}_{lm,\alpha}(r_{\alpha})), \end{aligned} \quad (68)$$

where

$$I'_3 = 2\int_0^{\pi/2}\int_0^{r_{\alpha}}\cos[r(\mathrm{k}_{P_1}-\mathrm{k}_{P_2})\cos\theta]J'_m(\kappa_{|L+nM_2|,N_2}r\sin\theta) \times J'_m(\kappa_{|L+nM_1|,N_1}r\sin\theta)\sin\theta r^2 d\theta dr, \quad (69)$$

$$I_4 = 2\int_0^{\pi/2}\int_0^{r_{\alpha}}\cos[r(\mathrm{k}_{P_1}-\mathrm{k}_{P_2})\cos\theta]J_m(\kappa_{|L+nM_2|,N_2}r\sin\theta) \times J_m(\kappa_{|L+nM_1|,N_1}r\sin\theta)(\sin\theta)^{-1}d\theta dr, \quad (70)$$

$$\gamma_{lm,\alpha} = (I_2^{*}I_1+I_1^{*}I_2)\dot{u}_{l,\alpha}u'_{l,\alpha}-I_2^{*}I_2\dot{u}_{l,\alpha}u_{l,\alpha}-I_1^{*}I_1\dot{u}'_{l,\alpha}u'_{l,\alpha}. \quad (71)$$

G. Dispersion curves and densities of states

The basis functions $\Psi_{PMN}(\mathrm{k},L)$ are everywhere continuous and differentiable, and the Rayleigh-Ritz variational principle is then easily applied. Expanding the electronic wave functions

$$\psi_i(\mathbf{r}|\mathrm{k},L) = \sum_{PMN}c_{i,PMN}(\mathrm{k},L)\Psi_{PMN}(\mathbf{r}|\mathrm{k},L) \quad (72)$$

and applying the variational principle then yield the secular equations

$$\det\| \langle \Psi_{P_2M_2N_2}|\hat{H}|\Psi_{P_1M_1N_1}\rangle|_{\mathrm{k},L}-E_i(\mathrm{k},L) \times|\langle \Psi_{P_2M_2N_2}|\Psi_{P_1M_1N_1}\rangle|_{\mathrm{k},L}\| = 0, \quad (73)$$

$$\sum_{P_1M_1N_1}[\langle \Psi_{P_2M_2N_2}|\hat{H}|\Psi_{P_1M_1N_1}\rangle|_{\mathrm{k},L}-E_i(\mathrm{k},L) \times|\langle \Psi_{P_2M_2N_2}|\Psi_{P_1M_1N_1}\rangle|_{\mathrm{k},L}]c_{i,PMN}(\mathrm{k},L) = 0. \quad (74)$$

The most important feature of the secular Eqs. (73) and (74) is that the Hamiltonian and overlap matrices are energy independent, which permits the simultaneous determination of the dispersion curves $E_i(\mathrm{k},L)$ and eigenvectors $c_{i,PMN}(\mathrm{k},L)$ for any particular values of the k and L.

In addition to the dispersion curves $E_i(\mathrm{k},L)$, the electronic structure of nanotubes can be characterized by energy dependences of the total and partial densities of states (DOSs). As to the total DOS, it is determined by the dispersion curves $E_i(\mathrm{k},L)$ only,

$$N(E) = \sum_i\sum_L\left[\frac{\partial E_i(\mathrm{k},L)}{\partial\mathrm{k}}\right]^{-1}, \quad (75)$$

but in order to obtain the partial DOS

$$N_l^{\alpha}(E) = \sum_i\sum_L Q_l^{\alpha}(i|\mathrm{k},L)\left[\frac{\partial E_i(\mathrm{k},L)}{\partial\mathrm{k}}\right]^{-1}, \quad (76)$$

one has to calculate a decomposition of the electron density $2|\psi_i(\mathbf{r}|\mathrm{k},L)|^2$ corresponding to the doubly occupied eigenstate $\psi_i(\mathbf{r}|\mathrm{k},L)$ with respect to atoms α and l. Here, $Q_l^{\alpha}(\mathrm{k},L)$ are the partial charges

$$Q_l^{\alpha}(i|\mathrm{k},L) = 2\sum_{P_2M_2N_2}\sum_{P_1M_1N_1} c^*_{i,P_2M_2N_2}(\mathrm{k},L)c^*_{i,P_1M_1N_1} \times(\mathrm{k},L)\frac{n}{h}(r_\alpha)^4(-1)^{n(M_2+M_1)}\exp\left\{i\left[\left(\mathrm{k}_{P_1}-\mathrm{k}_{P_2}-n(M_1-M_2)\frac{\omega}{h}\right)Z_\alpha+n(M_1 - M_2)\Phi_\alpha\right]\right\}\sum_{m=-l}^{l}[C^{J,L}_{M_2,N_2}J_{m-M_2}(\kappa_{|L+nM_2|,N_2}R_\alpha)+C^{Y,L}_{M_2,N_2}Y_{m-M_2}(\kappa_{|L+nM_2|,N_2}R_\alpha)][C^{J,L}_{M_1,N_1}J_{m-M_1}(\kappa_{|L+nM_1|,N_1}R_\alpha) + C^{Y,L}_{M_1,N_1}Y_{m-M_1}(\kappa_{|L+nM_1|,N_1}R_\alpha)]\frac{(2l+1)[(l-|m|)!]}{2[(l+|m|)!]}S^{P_2M_2N_2,P_1M_1N_1}_{lm,\alpha}(r_\alpha). \quad (77)$$

The partial DOS of the interspherical region is calculated from the equation

$$N_{IS}(E) = \sum_i\sum_L Q_{IS}(i|\mathrm{k},L)\left[\frac{\partial E_i(\mathrm{k},L)}{\partial \mathrm{k}}\right]^{-1}, \quad (78)$$

where

$$Q_{IS}(i|\mathrm{k},L) = 2\sum_{P_2M_2N_2}\sum_{P_1M_1N_1} c^*_{i,P_2M_2N_2}(\mathrm{k},L)c^*_{i,P_1M_1N_1} \times(\mathrm{k},L)\frac{n}{h}(r_\alpha)^4(-1)^{n(M_2+M_1)}\exp\left\{i\left[\left(\mathrm{k}_{P_1}-\mathrm{k}_{P_2}-n(M_1-M_2)\frac{\omega}{h}\right)Z_\alpha+n(M_1 - M_2)\Phi_\alpha\right]\right\}\sum_{m=-l}^{l}[C^{J,L}_{M_2,N_2}J_{m-M_2}(\kappa_{|L+nM_2|,N_2}R_\alpha)+C^{Y,L}_{M_2,N_2}Y_{m-M_2}(\kappa_{|L+nM_2|,N_2}R_\alpha)][C^{J,L}_{M_1,N_1}J_{m-M_1}(\kappa_{|L+nM_1|,N_1}R_\alpha) + C^{Y,L}_{M_1,N_1}Y_{m-M_1}(\kappa_{|L+nM_1|,N_1}R_\alpha)]\frac{(2l+1)[(l-|m|)!]}{2[(l+|m|)!]}I^{P_2M_2N_2,P_1M_1N_1}_{3,m\alpha}(r_\alpha). \quad (79)$$

It must be emphasized that the obtained equations for the dispersion curves and DOS are applicable not only to the carbon nanotubes but also to any tubule with rotational and helical symmetries. In the case of carbon tubule, there are only two terms in the sums over α in the equations for overlap and Hamiltonian integrals and partial charges. Moreover, the parameters R_α, r_α, $S_{lm,\alpha}$, $E_{l,\alpha}$, $\gamma_{lm,\alpha}$, and I_i $(i=1,\ldots,4)$ are the same for $\alpha=1$ and 2.

III. RESULTS OF CALCULATIONS

The convergence of the calculated band structures as a function of a number of basis functions was investigated. Figure 7 illustrates the results for the minimum optical energy gap E_{11} of the (11, 3) SWNT. One can see that about 150 functions produced convergence better then 0.01 eV. The same is true for other systems studied independent of the number of atoms in the translational unit cell.

By way of example, let us consider the total band structures and DOSs of the SWNTs (13, 0), (12, 2), (11, 3), (10, 5), (9, 6), and (8, 7) with virtually equal diameters $d=10.15\pm0.15$ Å, as well as the analogous data for the (7, 7) and (12, 4) SWNTs with slightly different $d=9.48$ and 10.70 Å, respectively. The SWNTs are known to be characterized by the "family index" $p=(n_1-n_2)$ mod 3. The tubules with $p=0$ are expected to be metallic or semimetallic, and those with $p=1$ and $p=2$ are semiconductors. Thus, there are chiral and achiral, semiconducting, semimetallic, and metallic SWNTs in this representative series.

Figure 8 shows the band structure of the chiral (11, 3) $p=1$ SWNT; the Γ and K points correspond to the Brillouin zone center (k=0) and boundary ($\mathrm{k}=\pi/h$), respectively.

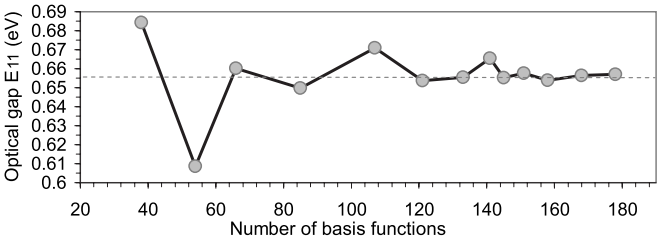

FIG. 7. LACW basis set convergence test for the (11,3) SWNT with 652 atoms in the translational unit cell.

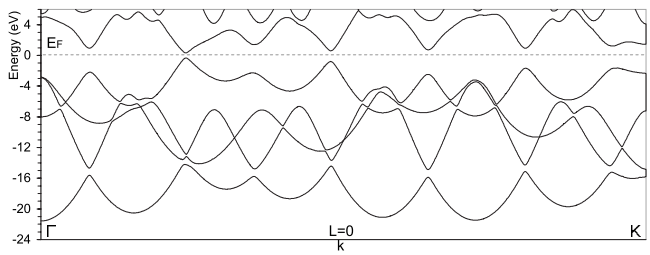

FIG. 8. Band structure of the (11,3) SWNT.

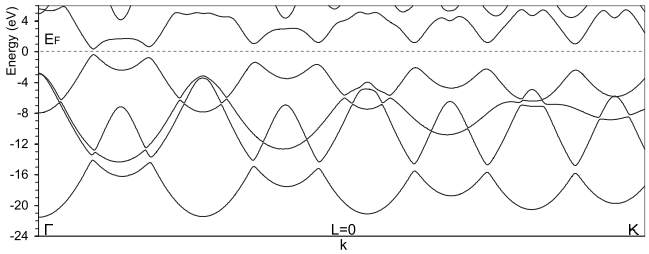

FIG. 9. Band structure of the (8,7) SWNT.

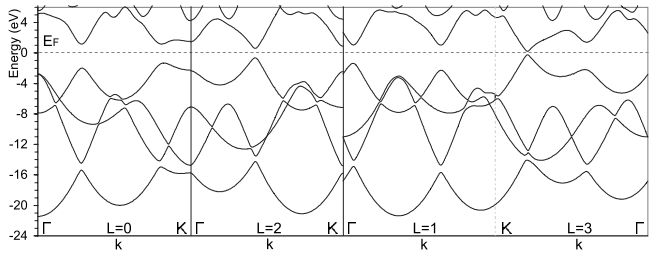

FIG. 11. Band structure of the (12,4) SWNT.

There is no rotational symmetry in this system. The translational unit cell contains as many as 652 atoms; however, the total band structure is seen to be very simple due to the account of the screw symmetry of the tubule. Particularly, there are only four dispersion curves in a valence band corresponding to the doubly occupied predominantly s, $p_{1\sigma}$, $p_{2\sigma}$, and p_{π} electronic states and only one low-energy unoccupied p_{π}^{*}-type dispersion curve in the conduction band. The same is true for the (8, 7) $p=1$ SWNT with 676 atoms per translational unit cell (Fig. 9).

According to the LACW data, the nanotubes (11, 3) and (8, 7) are the semiconductors with the direct energy gaps E_{11} equal to 0.656 at $k \approx 0.24(\pi/h)$ and 0.711 eV at $k \approx 0.089(\pi/h)$, respectively.

In the case of the (12, 2) $p=2$ SWNT, the largest common divisor of n_1 and n_2 indices is $n=2$; therefore, the structure of this tubule is characterized by the second order rotational axis C_2, and the eigenstates depend on the two quantum numbers, namely, the wave vector k and the rotational quantum number $L=0$ and 1 (Fig. 10).

As one goes from the (11, 3) and (8, 7) SWNTs to the (12, 2) tubule, the Brillouin zone is reduced approximately by one-half [Eq. (4)]. Now, there are four dispersion curves in the valence band and one curve in the low-energy region of the conduction band for every L value, and the band structure can be best demonstrated using the doubly repeated zone scheme. In this case, the dispersion curves for $L=1$ appear as the extensions of the curves for $L=0$, and the band diagrams of the (12, 2), (11, 3), and (8, 7) SWNTs become rather similar. In the (12, 2) tube, the $E_{11}=0.855$ eV corresponds to the direct transition between the states with $L=1$ about k point equal to $0.38(\pi/h)$.

In the case of the (12, 4) SWNT of the semiconducting $p=2$ family (Fig. 11), the integer L takes the values of 0,…,3. In the band structure, there are two pairs of continuous dispersion curves corresponding to $L=0$ and 2 and $L=1$ and 3, respectively, and the minimum gap $E_{11}=0.46$ eV corresponds to the direct transition between the states with $L=3$ at $k \approx 0.79(\pi/h)$.

Figures 12 and 13 show the band structures of the chiral (10, 5) $p=2$ and achiral zigzag (13, 0) $p=1$ SWNTs, which are characterized by the higher (5th and 13th) order rotational axes. In the repeated zone scheme, there are three and seven sets of dispersion curves, respectively. The bands for $n-L$ are the continuous extensions of the bands for L. The $E_{11}=0.816$ eV for the $L=2$ in the case of the (10, 5) tubule and 0.799 eV for the $L=9$ in the case of the (13, 0) SWNT. Note that, in the zigzag SWNTs, if one takes into account the translation symmetry only, the minimum gap E_{11} corresponds to the direct transition at the Brillouin zone $k=0$. With due account of the screw symmetry of the (13, 0) SWNT, the E_{11} corresponds to the point $\{k \approx 0.7,\ L=9\}$ (compare with the band diagrams of the screw and translational free electron models, Figs. 3 and 4).

Figure 14 shows the total DOSs of the five semiconducting SWNTs with virtually the same diameters $d=10.15 \pm 0.15$ Å. Although the band structures of these tubules look different, the total DOSs are very similar. An example of the partial DOSs of semiconducting tubule is presented in Fig. 15.

The (9, 6) SWNT with the rotational C_3 axis belongs to the $p=0$ family. As expected, there is no gap between the occupied and unoccupied π states (Fig. 16). Here, due to the SWNT curvature effects, an overlap of the bonding and antibonding π states equal to 0.15 eV takes place. In the repeated zone scheme, there are two sets of dispersion curves corresponding to $L=0$, 1, and 2, the curves for the $L=2$ being the extensions of the curves for the $L=1$.

Obviously, the armchair (7,7) SWNT is characterized by the metallic band structure with Fermi level at $L=0$ and $k \approx (2/3)(\pi/h)$ (Fig. 17).

As a final demonstration of the possibilities of this version of the LACW theory, we have calculated the band structure of the (100, 99) SWNT containing a total of 118 804 atoms

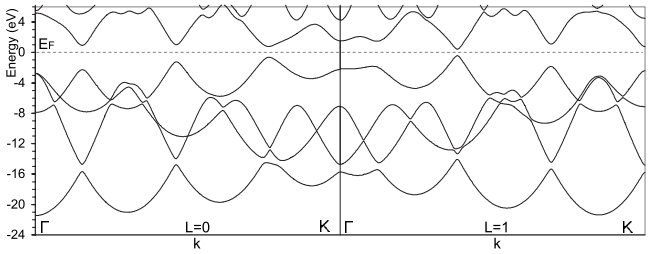

FIG. 10. Band structure of the (12,2) SWNT.

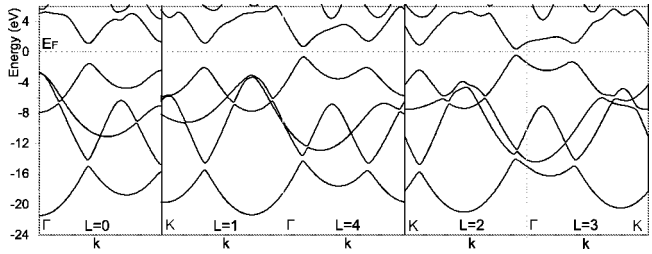

FIG. 12. Band structure of the (10,5) SWNT.

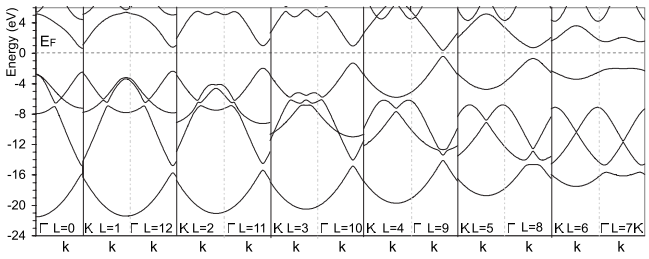

FIG. 13. Band structure of the (13,0) SWNT.

per translational unit cell (Fig. 18–20). Even for this system with huge unit cell, the band structure can be easily calculated and the results can be presented in the standard form of four continuous curves for the valence band plus one curve for the low-energy states of conduction band. This system is predicted to be the semiconductor with the gap $E_{11}=0.04$ eV near Brillouin zone center.

Finally, the highest occupied and lowest unoccupied LACW bands are in reasonable agreement with the standard π tight-binding data,[1]

$$\varepsilon(\mathrm{k},L) = \pm V_0\left[3 + 2\cos\left(\frac{n_1\mathrm{k} - 2\pi L p_1}{n}\right) + 2\cos\left(\frac{n_2\mathrm{k} - 2\pi L p_2}{n}\right) + 2\cos\left(\frac{(n_1+n_2)\mathrm{k} - 2\pi L(p_1+p_2)}{n}\right)\right]^{1/2}, \quad (80)$$

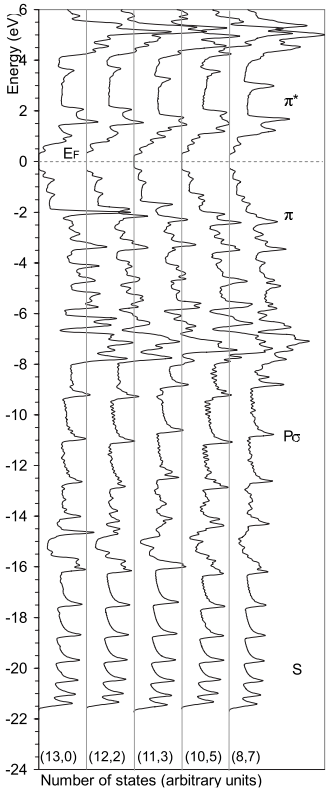

FIG. 14. Total DOSs of the SWNTs with $d=10.15\pm0.15$ Å.

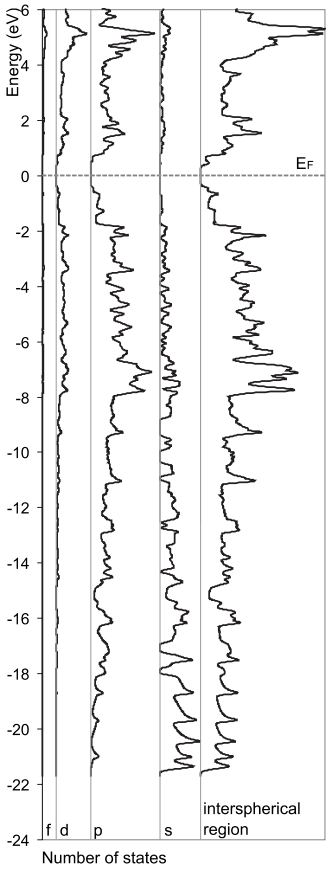

FIG. 15. Partial DOSs of the (12,2) tubule.

plotted using the same quantum numbers L and k (Figs. 21 and 22). Here, V_0 is the matrix element between the nearest-neighboring p_π-orbitals.

IV. CONCLUDING REMARKS

With account of rotational and helical symmetries, we developed a symmetry-adapted version of the LACW method. In this case, the *ab initio* theory becomes applicable to any SWNT. The obtained equations for the electron dispersion curves and DOS are suitable not only to the carbon systems but also to any tubule with these symmetries independent of the number and nature of atoms in the translational unit cell. The approximations are made in the sense of muffin-tin potentials and density functional theory only.

A further development of this theory is possible. In a full-potential version of the LACW method, we hope to

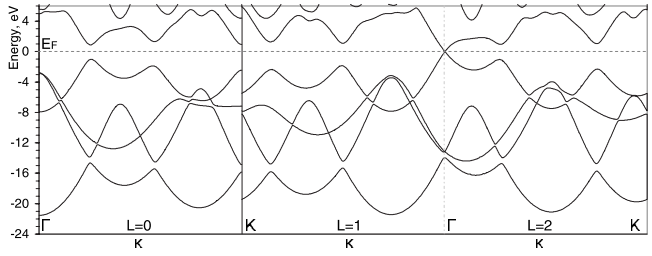

FIG. 16. Band structure of the (9,6) SWNT.

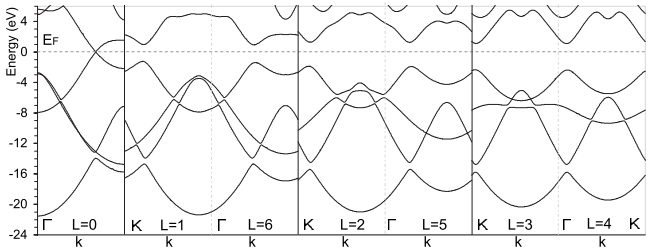

FIG. 17. Band structure of the (7,7) SWNT.

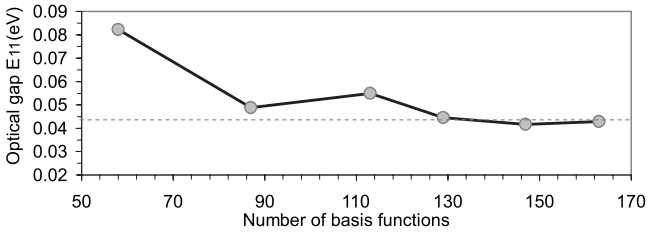

FIG. 18. LACW basis set convergence test for the (100,99) SWNT with 118 804 atoms in the translational unit cell.

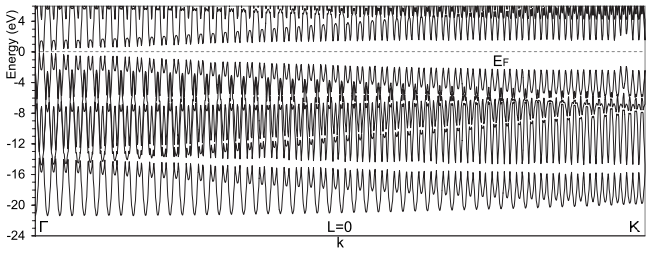

FIG. 19. Total band structure of the (100,99) SWNT.

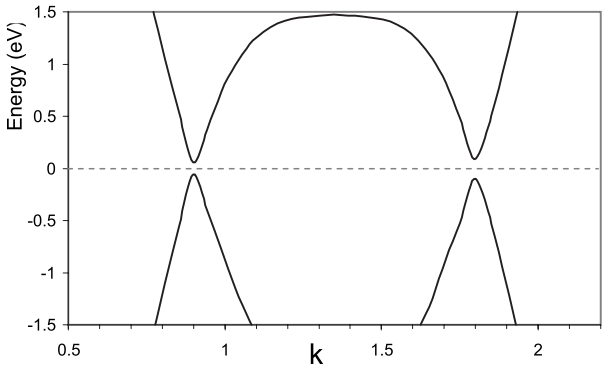

FIG. 20. Band structure of the (100,99) SWNT in the Fermi energy region.

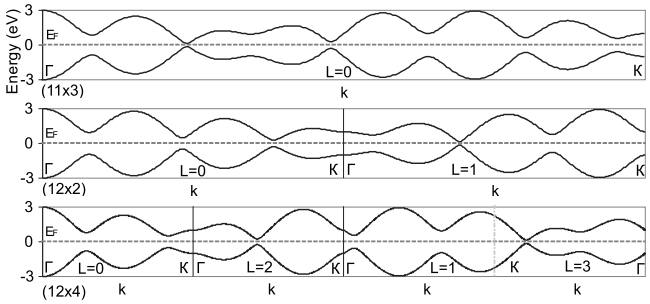

FIG. 21. Tight-binding π-band structures of semiconducting (11,3), (12,2), and (12,4) SWNTs plotted as the functions of two quantum numbers k and L.

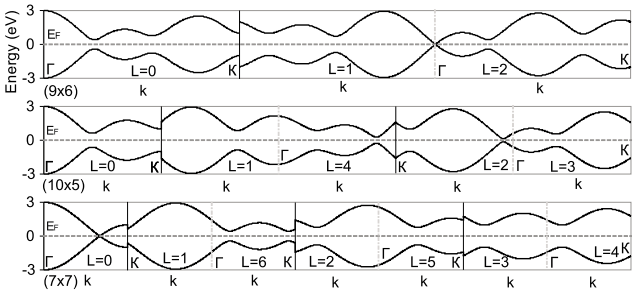

FIG. 22. Tight-binding π-band structures of two metallic (9,6) and (7,7) and one semiconducting (10,5) SWNTs plotted as functions of two quantum numbers k and L.

overcome the shortcomings of the muffin-tin approach. (For example, in the case of graphene, one can find both the (muffin-tin potential calculations and the full-potential studies of electron structure with due account of variations of electron density and potential in the interstitial regions[55]).

As to density functional theory, recall that DFT is designed to reproduce the total energies and not to calculate band structures. However, the DFT is empirically used to calculate electron structures; particularly, it is widely used in the *ab initio* LCAO and plane-wave pseudopotential calculations of the carbon SWNTs. In general, the DFT underestimates the band gaps of semiconductors and insulators;[56,57] therefore, we expect an overall increase in the values of the gaps calculated when considering quasiparticle corrections. These many-body effects between electrons can be taken into account within the GW approximation.[58,59] The GW approximation has been recently applied to $(n,0)$, $(5 \leqslant n \leqslant 9)$,[60,61] and (4,2) nanotubes,[23] and it was shown that the quasiparticle corrections to the DFT band structure are far from negligible in the case of the small-diameter tubules. Thus, an important improvement of the present approach can be made by combination of the LACW basis and GW approximation.

Finally, it should be noted that the symmetry-adapted generalized Bloch functions introduced in Ref. 1 for the π-electronic calculations were used recently for reducing the size of the Hamiltonian matrix for calculating the carbon SWNTs in the terms of the semiempirical tight-binding model using the atomic $2s$(C) and $2p$(C) basis[15,16] and in the *ab initio* model based on a many-body perturbation theory using the local basis of Gaussian orbitals centered on the C atoms.[62] In the latter case, as the first step of calculations, the ground state using the standard unsymmetrized plane-wave basis set was computed in the local density approximation, and the band states were calculated in Fourier space and then projected onto a set of basis functions of symmetrized Gaussian orbitals, the symmetry-adapted basis set being used only for the GW corrections.

Thus, our model uses the rotational and helical symmetries together with symmetry-adapted basis for the *ab initio* band structure calculation of nanotubes.

[1] C. T. White, D. H. Robertson, and J. W. Mintmire, Phys. Rev. B **47**, 5485 (1993).
[2] R. Saito, M. Fujita, G. Dresselhaus, and M. S. Dresselhaus, Phys. Rev. B **46**, 1804 (1992).
[3] R. Saito, M. Fujita, G. Dresselhaus, and M. S. Dresselhaus, Appl. Phys. Lett. **60**, 2204 (1992).
[4] N. Hamada, S. I. Sawada, and A. Oshiyama, Phys. Rev. Lett. **68**, 1579 (1992).
[5] J. W. Mintmire, B. I. Dunlap, and C. T. White, Phys. Rev. Lett. **68**, 631 (1992).
[6] R. Saito, A. Jorio, J. H. Hafner, C. M Lieber, M. Hunter, T. McClure, G. Dresselhaus, and M. S. Dresselhaus, Phys. Rev. B **64**, 085312 (2001).
[7] J. W. Mintmire, D. H. Robertson, and C. T. White, J. Phys. Chem. Solids **54**, 1835 (1993).
[8] J. W. Mintmire and C. T. White, Phys. Rev. Lett. **81**, 2506 (1998).
[9] A. Rubio, D. Sánchez-Portal, E. Artacho, P. Ordejón, and J. M. Soler, Phys. Rev. Lett. **82**, 3520 (1999).
[10] A. Hagen and T. Hertel, Nano Lett. **3**, 383 (2003).
[11] R. K. Vadapalli and J. W. Mintmire, Int. J. Quantum Chem. **106**, 2324 (2006).
[12] L. G. Bulusheva, A. V. Okotrub, D. A. Romanov, and D. Tomanek, J. Phys. Chem. A **102**, 975 (1998).
[13] G. Bussi, J. Menèndez, J. Ren, M. Canonico, and E. Molinari, Phys. Rev. B **71**, 041404(R) (2005).
[14] A. Hagen and T. Hertel, in *Molecular Nanostructures: XVII International Winterschool/Euroconference on Electronic Properties of Novel Materials*, AIP Conf. Proc. No. 685 edited by H. Kuzmany, J. Fink, M. Mehring, S. Roth (AIP, Melville, NY, 2003) p. 193.
[15] V. N. Popov, New J. Phys. **6**, 17 (2004).
[16] V. N. Popov and L. Henrard, Phys. Rev. B **70**, 115407 (2004).
[17] H. Ajiki and T. Ando, J. Phys. Soc. Jpn. **62**, 1255 (1993).
[18] H. Ajiki and T. Ando, J. Phys. Soc. Jpn. **65**, 505 (1996).
[19] K. V. Christ and H. R. Sadeghpour, Phys. Rev. B **75**, 195418 (2007).
[20] X. Blase, L. X. Benedict, E. L. Shirley, and S. G. Louie, Phys. Rev. Lett. **72**, 1878 (1994).
[21] S. Reich, C. Thomsen, and P. Ordejón, Phys. Rev. B **65**, 155411 (2002).
[22] S. Reich, J. Maultzsch, C. Thomsen, and P. Ordejón, Phys. Rev. B **66**, 035412 (2002).
[23] J.-C. Charlier, Ph. Lambin, and T. W. Ebbesen, Phys. Rev. B **54**, R8377 (1996).
[24] M. Machón, S. Reich, C. Thomsen, D. Sánchez-Portal, and P. Ordejón, Phys. Rev. B **66**, 155410 (2002).
[25] A. G. Marinopoulos, L. Reining, A. Rubio, and N. Vast, Phys. Rev. Lett. **91**, 046402 (2003).
[26] V. Zólyomi and J. Kürti, Phys. Rev. B **70**, 085403 (2004).
[27] I. Cabria, J. W. Mintmire, and C. T. White, Phys. Rev. B **67**, 121406(R) (2003).
[28] O. Dubay, G. Kresse, and H. Kuzmany, Phys. Rev. Lett. **88**, 235506 (2002).
[29] Z. M. Li, Z. K. Tang, H. J. Liu, N. Wang, C. T. Chan, R. Saito, S. Okada, G. D. Li, J. S. Chen, N. Nagasawa, and S. Tsuda, Phys. Rev. Lett. **87**, 127401 (2001).
[30] H. J. Liu and C. T. Chan, Phys. Rev. B **66**, 115416 (2002).
[31] J. Kürti, V. Zólyomi, M. Kertesz, G. Sun, R. H. Baughman, and H. Kuzmany, Carbon **42**, 971 (2004).
[32] G. Sun, M. C. Nicklaus, and M. Kertesz, in *Encyclopedia of Nanoscience and Nanotechnology*, edited by J. A. Schwarz, C. Contescu, and K. Putyera (Dekker, New York, 2004), p. 3605.
[33] T. Miyake and S. Saito, Phys. Rev. B **68**, 155424 (2003).
[34] C.-K. Skylaris, P. D. Haynes, A. Mostofi, and M. C. Payne, J. Chem. Phys. **122**, 084119 (2005).
[35] P. N. D'yachkov, O. M. Kepp, and A. V. Nikolaev, Dokl. Chem. **365**, 67 (1999); in *Science and Application of Nanotubes*, edited by D. Tomanek and R. J. Enbody (Kluwer Academic, Dordrecht/Plenum, New York, 2000), 77.
[36] P. N. D'yachkov and D. V. Kirin, Dokl. Phys. Chem. **369**, 326 (1999); in *Proceedings of the School and Workshop on Nanotubes and Nanostructures, Santa Margherita di Pula, CA, Italy, 2000*, edited by S. Bellucci (SIF, Bologona, 2001), Vol. 74, p. 203.
[37] P. N. D'yachkov, in *Encyclopedia of Nanoscience and Nanotechnology*, edited by H. S. Nalwa (American Scientific, Valencia, CA, 2004), Vol. 1, p. 191.
[38] O. K. Andersen, Phys. Rev. B **12**, 3060 (1975).
[39] D. D. Koelling and G. O. Arbman, J. Phys. F: Met. Phys. **5**, 2041 (1975).
[40] D. J. Singh, *Planewaves, Pseudopotentials and the LAPW Method*. (Kluwer, Boston, 1994).
[41] P. N. D'yachkov, H. Hermann, and D. V. Kirin, Appl. Phys. Lett. **81**, 5228 (2002).
[42] P. N. D'yachkov and H. Hermann, J. Appl. Phys. **95**, 399 (2004).
[43] P. N. D'yachkov and D. V. Makaev, Phys. Rev. B **74**, 155442 (2006).
[44] D. V. Makaev and P. N. D'yachkov, JETP Lett. **84**, 397 (2006).
[45] A. V. Nikulkina and P. N. D'yachkov, Russ. J. Inorg. Chem. **49**, 430 (2004).
[46] A. Yu. Golovacheva and P. N. D'yachkov, JETP Lett. **82**, 834 (2005).
[47] P. N. D'yachkov and D. V. Makaev, Phys. Rev. B **71**, 081101(R) (2005).
[48] D. V. Makaev and P. N. D'yachkov, Dokl. Phys. Chem. **402**, 109 (2005).
[49] J. C. Slater, *Quantum Chemistry of Molecules and Crystals* (McGraw-Hill, New York, 1974), Vol. 4.
[50] P. Hohenberg and W. Kohn, Phys. Rev. **136**, B864 (1964).
[51] W. Kohn and L. J. Sham, Phys. Rev. **140**, A1133 (1965).
[52] G. N. Watson, *Treatise on the Theory of Bessel Functions*, 2nd ed. (Cambridge University Press, New York, 1966).
[53] G. A. Korn and T. M. Korn, *Mathematical Handbook for Scientists and Engineers* (McGraw-Hill, New York, 1961).
[54] C. T. White and J. W. Mintmire, J. Phys. Chem. B **109**, 52 (2005).
[55] R. C. Tatar and S. Rabii, Phys. Rev. B **25**, 4126 (1982).
[56] M. S. Hybertsen and S. G. Louie, Phys. Rev. B **34**, 5390 (1986).
[57] M. Grüning, A. Marini, and A. Rubio, Phys. Rev. B **74**, 161103(R) (2006).
[58] L. Hedin, Phys. Rev. **139**, A796 (1965).
[59] P. Sun and G. Kotliar, Phys. Rev. Lett. **92**, 196402 (2004).
[60] T. Miyake and S. Saito, Phys. Rev. B **68**, 155424 (2003).
[61] T. Miyake and S. Saito, Phys. Rev. B **72**, 073404 (2005).
[62] E. Chang, G. Bussi, A. Ruini, and E. Molinari, Phys. Rev. B **72**, 195423 (2005).